Constraining Regional Hydrological Sensitivity over Tropical Oceans

Under review at GRL (submitted on Mar. 25 2024)

Jie He[1]

Yi Deng[1]

Boniface Fosu[2,3]

Yen-Heng Lin[3]

Kezhou Lu[1]

1. School of Earth and Atmospheric Sciences, Georgia Institute of Technology, GA, United States

2. Department of Geosciences, Mississippi State University, Mississippi State, MS, United States

3. Northern Gulf Institute, Mississippi State University, Mississippi State, MS, United States

Abstract

Regional hydrological sensitivity (i.e., precipitation change per degree local surface warming) contributes substantially to the uncertainty in future precipitation projections over tropical oceans. By applying a 2-mode model that dissects precipitation changes from sea surface temperature (SST) changes and those from SST gradient changes, we find that the relationship between relative precipitation (i.e., precipitation divided by the basin mean precipitation) and relative SST (i.e., SST minus the tropical mean SST) and that between relative precipitation and SST gradient remain virtually constant during climate change. This means that regional hydrological sensitivity can be constrained by the present-day SST-precipitation relationship. We report that climate models systematically underestimate precipitation sensitivity to local relative SST changes. However, such a bias has limited impact on tropical precipitation changes, which are primarily associated with

SST gradient changes. The sensitivity of precipitation to SST gradient changes is well represented by the multi-model average.

Key Points

- Regional hydrological sensitivity is an important source of uncertainty in rainfall projections over tropical oceans.
- Regional hydrological sensitivity can be constrained by components of rainfall-temperature relationship that stay constant during warming.
- Regional hydrological sensitivity is linked to surface temperature gradients and this link is well captured by the multi-model average.

Plain Language Summary

Understanding how precipitation will change over tropical oceans is important because these changes influence the atmospheric circulation, which in turn affects the global climate and weather patterns. Climate models disagree on their projections of precipitation changes over tropical oceans in part due to a lack of understanding on how precipitation should respond to a given amount of local surface warming. We find that the sensitivity of precipitation to future changes in local sea surface temperature (which is commonly referred to as regional hydrological sensitivity) largely depends on how precipitation varies with the local sea surface temperature in the present-day climate. This allows us to constrain the projected precipitation sensitivity to future warming based on the observed present-day precipitation-sea surface temperature relationship. We find that the sensitivity of precipitation to local warming primarily depends on how such warming affects the

spatial gradient of surface temperature. This aspect of precipitation sensitivity is well represented by the multi-model average but differs substantially among individual climate models.

1. Introduction

Tropical precipitation is a main component of the global hydrological cycle. Both tropical land and oceanic precipitation changes have far-reaching implications on the global climate system via atmospheric teleconnections (e.g., Chen et al., 2020; Lu et al., 2023). The projection of future tropical precipitation is highly uncertain at regional scales (e.g., McSweeney & Jones, 2013). The uncertainty in regional precipitation over tropical oceans is often attributed to the uncertainty in sea surface temperature (SST) changes (Kent et al., 2015; Ma & Xie, 2013), because precipitation changes generally follow local SST changes (S.-P. Xie et al., 2010). But SST is only half of the equation. Chadwick (2016) showed that a considerable portion of the inter-model spread in tropical precipitation changes persist when the models are driven by the same SST changes (their Fig. 5, reproduced in Supplementary Figs. 1a, b). This suggests that the uncertainty in regional precipitation changes (δP) is not only associated with local SST changes (δSST), but likely precipitation sensitivity to local SST changes ($\delta P/\delta SST$) as well. However, regional hydrological sensitivity (which describes precipitation change per degree local surface temperature change) has not been thoroughly studied.

On the other hand, there has been great interest surrounding the global and tropical mean hydrological sensitivity due to its substantial variance among climate models (DeAngelis et al., 2015; Su et al., 2017; Watanabe et al., 2018; J. Zhang & Huang, 2023). The tropical mean hydrological sensitivity (often calculated as the percentage change in tropical mean precipitation per degree tropical mean surface warming) varies by roughly a factor of three among the Coupled

Model Intercomparison Project (CMIP) models (He & Soden, 2015). Means to constrain the projected tropical mean hydrological sensitivity have been explored in recent studies (Ham et al., 2018; Park et al., 2022). In comparison, regional hydrological sensitivity has received far less attention. However, because the broader impacts of tropical precipitation changes depend more on the regional distribution rather than the tropical mean of such changes (Lu et al., 2023), understanding regional hydrological sensitivity is important from both scientific and pragmatic points of view.

While hydrological sensitivity to future warming has been underexplored, it is useful to review precipitation sensitivity to internal SST variations, where some progress has been made in recent years. He et al. (2018) found that the equations that determine the precipitation sensitivity to internal SST variability are the same as those governing the climatological mean SST-precipitation relationship. This means that the response of precipitation per degree internal SST variation is the same as the variation in climatological precipitation per degree climatological SST variation (i.e., the slope of climatological precipitation in SST space, Figs. 1a, b). The implication of such a finding is that during internal climate variations, changes in SSTs result in a geographical reshuffling of convective and non-convective areas while the SST-precipitation relationship remains constant. In addition, because internal precipitation variability is driven by a multitude of factors, a major challenge in quantifying precipitation sensitivity to internal SST variability is to derive a physically meaningful relationship between precipitation anomalies and SST anomalies (Graham & Barnett, 1987; Lau et al., 1997; C. Zhang, 1993). The constancy in SST-precipitation relationship during internal climate variations allows us to constrain models' precipitation sensitivity to internal SST anomalies by using the observed climatological SST-precipitation relationship. It was shown that climate models systematically underestimate precipitation sensitivity to internal and seasonal SST variations (Good et al., 2020).

Although precipitation responds differently to internal and anthropogenic SST variations (e.g., Kramer & Soden, 2016), it has been reported that certain aspects of SST-precipitation relationship could remain constant during climate change. For example, Johnson & Xie (2010) examined the tropical mean SST-precipitation relationship and argued that the present-day and future relationship between precipitation and relative SST (SST_{rel}, defined as SST minus the tropical mean SST) is roughly the same (their Fig. 3a). But this appears to be an oversimplification when the three tropical basins are examined separately. As shown in Figure 1b, the Pacific precipitation is projected to shift markedly upwards in SST_{rel} space, while the other two basins exhibit moderate changes. The inter-basin differences in precipitation changes were recently attributed to the thermodynamic intensification of boundary-layer moisture transport (He et al., 2024). However, much of the changes in precipitation in SST_{rel} space appear to be associated with changes in the basin mean precipitation. If we divide precipitation by the basin mean precipitation, which we refer to as relative precipitation (P*), P* appears largely constant within each basin (Fig. 1d). Therefore, we hypothesize that the relationship between P* and SST_{rel} does not change under warming. If valid, this would allow us to derive the sensitivity of P* to local SST_{rel} changes based on the present-day SST_{rel}-P* slope.

We will test the hypothesis by deriving an SST-based model of present-day and future precipitation. This was often done by fitting precipitation to some nonlinear function of SST (e.g., Good et al., 2020; He et al., 2018; Neelin & Held, 1987). However, precipitation is affected by not only the amplitude but also the spatial gradient of SST (Back & Bretherton, 2009b; Lindzen & Nigam, 1987). The latter drives convection by inducing surface wind convergence (SC) and is a dominant driver of future precipitation changes in tropical oceans (Duffy et al., 2020). These processes can be quantified by a 2-mode model where precipitation is expressed as a function of SST and SC (as a proxy for the effect of SST gradients, Back & Bretherton, 2009a; Duffy et al., 2020). Here, we will introduce an upgraded version of the 2-mode model (Section 3). We will then use it to quantify and constrain the sensitivity of P* to SST_{rel} changes ($\partial P^*/\partial SST_{rel}$) and SST gradient changes ($\partial P^*/\partial SC$, Section 4). We will finally discuss the implications of $\partial P^*/\partial SST_{rel}$ and $\partial P^*/\partial SC$ for regional hydrological sensitivity ($\partial P/\partial SST$) and tropical precipitation projections (Section 5).

2. Data

We quantify $\partial P^*/\partial SST_{rel}$ and $\partial P^*/\partial SC$ over tropical (20°S-20°N) oceans in both observations and CMIP6 simulations. All datasets are interpolated onto a common 1° by 1° horizontal grid and a 19-level pressure coordinate before they are analyzed. We take monthly mean data but only analyze the seasonally varying climatological means.

The observed SST data is a merged product based on the Hadley Centre SST dataset version 1 and the National Oceanic and Atmospheric Administration optimum interpolation SST analysis version 2 (Hurrell et al., 2008). The data ranges from 1979 to 2021 and is archived at 1° resolution. To account for the uncertainty in individual precipitation observations, we average three widely used precipitation datasets: 1) the Global Precipitation Climatology Project (GPCP) data version 2 from 1979 to 2021 at 2.5° resolution (Adler et al., 2003), 2) the Climate Prediction Center Merged Analysis of Precipitation (CMAP) data from 1979 to 2021 at 2.5° resolution (P. Xie & Arkin, 1997), and 3) the Tropical Rainfall Measuring Mission Project (TRMM) 3B43 data version 7 from 1998 to 2019 at 0.25° resolution (Huffman et al., 2010). While the results presented in this paper are based on the average of the three precipitation observations, our conclusions do not change when individual precipitation datasets are used instead.

To quantify the impacts of SST amplitude and SST gradients on the observed precipitation (see Section 3), we use 3D atmospheric variables, including horizontal and vertical winds and dry static energy (calculated from air temperature and geopotential height). These variables are taken from reanalysis data during the period of 1979 to 2021. To minimize the effect of uncertainty within individual datasets, we average three widely used reanalysis datasets: 1) ERA5 (the 5th generation of the European Centre for Medium-Range Weather Forecasts reanalysis) on a 30km horizontal grid and 137 vertical levels (Hersbach et al., 2020), 2) NCEP/DOE-II (the National Center for Environmental Prediction and Department of Energy Reanalysis II) at 2.5° resolution with 17 vertical levels (Kanamitsu et al., 2002), and 3) JRA-55 (the Japanese 55-year Reanalysis) at roughly 1° resolution with 37 vertical levels (KOBAYASHI et al., 2015).

We analyze two CMIP6 simulations (Eyring et al., 2016) by drawing the 43 models (Supplementary Table 1) that provide all necessary variables. The historical simulation is driven by historical estimates of radiative forcing and land use. We use the last 30 years (1985-2014) of the historical simulation to evaluate models against observations and to provide a baseline for future changes. The projected future climate is calculated based on the last 30 years (2071-2100) of the ssp585 simulation. ssp585 represents the upper boundary of the range of emission scenarios included in CMIP6, and its radiative forcing reaches 8.5 W/m^2 by 2100.

3. 2-mode model

We apply a 2-mode model to dissect precipitation driven by SST amplitude and SST gradient. The 2-mode model was originally created by Back & Bretherton (2009a). "2-mode" refers to the fact that tropical precipitation is primarily associated with either a shallow or a deep vertical velocity profile (Figs. 1e, f). The shallow mode features maximum updraft in the boundary layer. The bottom-heavy structure is associated with strong boundary layer wind convergence which is driven by low-level pressure gradients that result from the gradients of the underlying SSTs (Back & Bretherton, 2009b; Lindzen & Nigam, 1987). The shallow mode is the main form of precipitation in the Eastern Pacific convergence zone and is closely related to SC. The deep mode peaks in the upper troposphere and can be attributed to atmospheric instability driven by a high amount of near surface moist static energy (Back & Bretherton, 2009a). It is therefore strongest in the warm pool regions but can also be affected by SST gradients, which can increase low-level moist static energy by generating moisture convergence (Duffy et al., 2020). Our 2-mode model largely follows the latest published version from Duffy et al. (2020), but with a few modifications that lead to substantial improvements. We will use the 2-mode model to simulate relative precipitation, which is the constrainable component of tropical precipitation changes (as we will later show). The main steps of the 2-mode model are outlined below. We direct the readers to Back & Bretherton (2009a) and Duffy et al. (2020) for details of the calculation, while pointing out the modifications made herein.

Analysis of the atmospheric energy budget reveals that the spatial distribution of tropical precipitation is determined mainly by the column integrated vertical advection of dry static energy (Back & Bretherton, 2009a):

$$LP^* = {\langle \omega \frac{\partial s}{\partial p} \rangle}\Big/{[P]} + r \qquad (1)$$

where L is the latent heat of condensation, P is precipitation, $P*$ is relative precipitation (i.e., P divided by the basin mean precipitation, $[P]$), ω is pressure velocity, s is dry static energy, p is pressure, and $\langle\,\rangle$ is a pressure weighted vertical integral over an atmospheric column. The residual term (r) is the sum of horizontal advection of s, eddy transport of s, surface sensible heat flux, and the atmospheric radiative cooling (i.e., the difference between surface and top of the atmosphere radiation), all normalized by $[P]$. r has little spatial variation and is roughly equal to 1. We calculate r as the difference between LP^* and $\langle\omega \frac{\partial s}{\partial p}\rangle / [P]$.

Equation 1 links precipitation to vertical velocity (ω); the latter is dissected into a deep mode (subscript d) and a shallow mode (subscript s):

$$\omega \approx o_d\Omega_d + o_s\Omega_s \qquad (2)$$

where $\Omega(p)$ describes the vertical profiles of each mode and $o(x,y,t)$ describes the spatial and seasonal variation. The deep and shallow modes are determined based on a linear combination of the first two EOF modes of ω, while ensuring that the shallow mode has zero surface convergence and the deep mode is orthogonal to the shallow mode (Back & Bretherton, 2009a). While in previous 2-mode models, the dissection of the deep and shallow modes is done by using data of the entire tropical oceans, we do it separately for individual basins. This is motivated by the fact that the vertical profiles of ω differ substantially among basins. The Indian (Atlantic) basin has the largest (smallest) peaks in both deep and shallow modes and such differences are more pronounced in reanalysis than the CMIP6 multi-model mean (Figs. 1e, f). The reason for the inter-basin differences is unclear but is likely associated with inter-basin differences in SST, humidity, and land influences (He et al., 2024).

Following previous 2-mode models, we also separate r into deep and shallow modes by linear multiple regression:

$$r \approx o_d R_d + o_s R_s + R_0 \qquad (3)$$

where R_d, R_s, and R_0 are constant regression coefficients. While it is unclear how r is physically linked to o_d and o_s, Equation 3 is calculated solely for the mathematical purpose that both terms on the rhs of Equation 1 are dissected into deep and shallow modes. Combining Equations 1-3 yields the deep and shallow modes of P^*: $LP^* \approx LP_d^* + LP_s^* + R_0$, where $LP_d^* = \left(\langle \Omega_d \frac{\partial s}{\partial p} \rangle \Big/ [P] + R_d \right) o_d$ and $LP_s^* = \left(\langle \Omega_s \frac{\partial s}{\partial p} \rangle \Big/ [P] + R_s \right) o_s$. Spatial patterns of the deep and shallow precipitation are shown in Supplementary Figure 2.

The shallow mode of P^* is related to SST gradients by linear regression: $P_s^* \approx A_s SC + C_s$, where A_s and C_s are regression coefficients. $SC = -\nabla(u_{925hPa}, v_{925hPa})$, where u_{925hPa} and v_{925hPa} are 925 hPa horizontal winds. Alternatively, the effect of SST gradients can be estimated by the Laplacian of SST, but ∇^2SST is substantially worse at capturing the spatial features of precipitation compared to SC (Back & Bretherton, 2009a; Duffy et al., 2020).

The deep mode of P* is related to SST amplitude and SST gradients by multiple regression: $P_d^* \approx b \times \exp(a \times SST_{rel}) + A_d SC + C_d$, where a, b, A_d and C_d are regression coefficients. The coefficients are determined via a nonlinear least squares analysis based on the trust region method (Conn et al., 2000). Here, we make two modifications with respect to previous 2-mode models. First, previous models estimated coefficients (i.e., a, b, A_d, and A_s) by using data of the entire tropical oceans. This yielded spatially uniform parameters. But as shown in Figures 1c and 1d, the SST_{rel}-P* relationship varies substantially among basins, which indicates that the parameters may be basin dependent. The inter-basin differences in hydrological sensitivity were investigated in He et al. (2024) and were attributed to inter-basin differences in boundary-layer relative humidity. To account for the inter-basin variations, we estimate all coefficients separately for individual basins.

Second, previous 2-mode models assumed that the SST_{rel}-driven P_d is zero below a certain convection threshold and grows linearly with SST above the convection threshold. This appears somewhat inconsistent with the actual SST-P relationship, which shows gradual and nonlinear precipitation growth throughout the SST space (Figs. 1a, b). Therefore, we use an exponential function (i.e., $b \times \exp(a \times SST_{rel})$) to represent the SST_{rel}-driven P_d. On the other hand, we are dealing with two SST_{rel} parameters (i.e., a and b). The two parameters both contribute positively to the SST_{rel}-driven P_d but are negatively correlated among models (Fig. 2a). To simplify the interpretation of the parameters, we set b constant while only allowing a to vary among models. Specifically, we estimate both a and b for the observations. But for CMIP6 models, b is prescribed for each basin as the observed values for both present-day and future simulations. The reason for making a (instead of b) the effective SST_{rel} parameter is twofold. First, making a constant across models instead would result in slightly greater root mean squared error (rmse) for the estimated precipitation, suggesting that the inter-model variation in the SST_{rel}-P_d relationship is more associated with a. Second, our choice is consistent with Good et al. (2020) who also used an exponential function to describe the SST-driven precipitation and proposed that precipitation sensitivity to SST should be represented by the coefficient within the exponent. Nevertheless, whether a or b is made the effective SST_{rel} parameter does not affect our conclusions.

The above modifications result in substantial improvements in the 2-mode model (Figs. 3a-d). The rmse for the estimated observed precipitation is 0.89 mm/day, compared to the rmse of 2.30 mm/day in Back & Bretherton (2009a) and 2.08 mm/day in Duffy et al. (2020). The improvement is almost entirely due to the incorporation of the inter-basin differences in Ω profiles and sensitivity parameters. If the inter-basin variations are ignored, the rmse would increase to 2.03 mm/day, which is similar to previous versions.

The 2-mode model dissects $P*$ into components driven by SST amplitude and SST gradients (*SC*):

$$P^* \approx P^*(SST) + P^*(SC) + C_d + C_s + {R_0}/{L} \qquad (4),$$

where $P^*(SST) = b \times \exp(a \times SST_{rel})$, and $P^*(SC) = (A_d + A_s)SC$. As shown in Figures 3e-h, spatial variations in tropical precipitation are more associated with *SC* than SST_{rel}. Particularly in the Atlantic basin, the impact of SST_{rel} is very small. This is likely because the Atlantic basin is colder than the other two basins and the effect of SST amplitude only becomes significant at high SSTs (He et al., 2018).

The 2-mode model captures the CMIP6 multi-model mean $P*$ changes reasonably well (Figs. 4a, b). The most notable inconsistencies appear in the Equatorial regions, which is also an issue for the previous 2-mode model (Fig. 2 of Duffy et al., 2020). The multi-model mean rmse for the estimated precipitation changes is brought down to 0.49 mm/day compared to the 0.62 mm/day of Duffy et al. (2020). Consistent with Duffy et al. (2020), *SC* plays a substantially greater role in the projected tropical precipitation changes than SST_{rel} (Figs. 4c, d). Note that Duffy et al. (2020) attributed a portion of precipitation changes to the "wet-get-wetter" effect (their Fig. 2d), which is absent here because we only consider changes in $P*$ rather than *P*.

4. Regional precipitation sensitivity to anthropogenic SST_{rel} and SC changes

The present-day and future parameters are not only highly correlated among GCMs but are also similar in amplitude (Figs. 3b, c). Parameter *a* tends to be slightly lower at present-day, while parameter A ($A = A_d + A_s$) is somewhat higher at present-day. Nevertheless, the differences between present-day and future parameters are substantially smaller than the parameters themselves. In Figure 4e, we estimate P* changes by the present-day parameters to calculate P* in both historical and ssp585 simulations. The resulting P* changes are very similar to those in Figure 4b. This means that the present-day and future P* can be represented by the same 2-mode model with only differences in SST_{rel} and SC. This confirms our hypothesis that the SST_{rel}-P* and SC-P* relationships are essentially constant during climate change, while changes in P* are mainly associated with the geographic reshuffling of SST_{rel} and SC. To further confirm this point, we show that P* changes little in SST_{rel}-SC space (Supplementary Figure 3).

Because the present-day and future parameters are roughly the same, we can obtain P* sensitivity to local SST_{rel} and SC changes by calculating the SST_{rel} and SC derivatives of Equation 4: ${\partial P^*}/{\partial SST_{rel}} = ab \times \exp(a \times SST_{rel})$, and ${\partial P^*}/{\partial SC} = A$.

Because we hold parameter b constant across models, ${\partial P^*}/{\partial SST_{rel}}$ is a function of a and SST_{rel}. By comparing a of GCMs and observations, we find that ${\partial P^*}/{\partial SST_{rel}}$ is underestimated by most GCMs (Fig. 2b). This is consistent with Good et al. (2020), who reported systematic underestimations of precipitation sensitivity to internal and seasonal SST variations by CMIP models. In addition, there is substantial inter-model variation in a. The uncertainty in a has greater impacts on ${\partial P^*}/{\partial SST_{rel}}$ at higher SSTs. For example, the Pacific ${\partial P^*}/{\partial SST_{rel}}$ varies by a factor of 1.7 among GCMs for $SST_{rel}=0$ and a factor of 3.4 for $SST_{rel}=2^{o}C$ (equivalent to present-day SST of roughly 29 ^{o}C).

The observational estimate of ${\partial P^*}/{\partial SC}$ is well represented by the CMIP6 multi-model mean (Fig. 2c). While there are no systematic biases in ${\partial P^*}/{\partial SC}$, there is considerable inter-model variance. $\partial P^*/\partial SC$ varies by a factor of 2.1, 2.2, and 2.8 for the Indian, Pacific, and Atlantic basin, respectively.

How does biases and uncertainties in $\partial P^*/\partial SST_{rel}$ and $\partial P^*/\partial SC$ affect the projection of tropical precipitation? Because the multi-model mean $\partial P^*/\partial SC$ biases are small and because most of the P* changes are associated with SC, the multi-model mean P* changes are not much affected by biases in $\partial P^*/\partial SST_{rel}$. In Figure 4f, we estimate P* changes by using observational parameters and found very similar results to those estimated with GCMs' historical parameters (Fig. 4e). To assess how inter-model variations in $\partial P^*/\partial SST_{rel}$ and $\partial P^*/\partial SC$ affect P* changes, we recalculate the multi-model mean P* changes in the 2-mode model by using parameters from GCMs with the lowest and highest $\partial P^*/\partial SST_{rel}$ and $\partial P^*/\partial SC$ (Figs. 4g-j). While the impact of inter-model variations in $\partial P^*/\partial SST_{rel}$ appears moderate, that of $\partial P^*/\partial SC$ is substantially greater. The impact of $\partial P^*/\partial SC$ can also be appreciated by comparing P* changes in individual GCMs, as models with the highest $\partial P^*/\partial SC$ project substantially more spatially varying P* changes (Supplementary Figure 4). These results suggest that constraining $\partial P^*/\partial SC$ should help greatly to reduce the uncertainty in tropical precipitation changes.

5. Discussions

$\partial P^*/\partial SST_{rel}$ and $\partial P^*/\partial SC$ are quantitatively linked to regional hydrological sensitivity (i.e., $\partial P/\partial SST$). Knowing $\partial P^*/\partial SST_{rel}$ and $\partial P^*/\partial SC$, one can easily obtain ∂P and then $\partial P/\partial SST$, if $[P]$ and changes in surface conditions (i.e., ∂SST and ∂SC) are also known.

(Uncertainties in [P] contribute little to the uncertainty in regional precipitation changes as demonstrated in Supplementary Figures 1c, d.) On the other hand, a separate discussion of $\partial P^*/\partial SST_{rel}$ and $\partial P^*/\partial SC$ is helpful for the physical interpretation of regional hydrological sensitivity. The traditionally defined hydrological sensitivity interprets regional precipitation changes as responses to changes in local SST amplitude (i.e., $\partial P = \partial P/\partial SST \times \partial SST$). However, this can be misleading because regional precipitation changes over tropical oceans are primarily driven by ∂SC, which are associated with SST gradients rather than the amplitude of local SSTs.

In the 2-mode model, the SST-driven and SC-driven P_d is estimated by multiple nonlinear regression. This can be potentially problematic because SST_{rel} and SC are not entirely independent (with a spatial correlation of 0.6 in observations and reanalysis). Therefore, the effects of SST amplitude and SST gradients may not be cleanly separated by statistical methods. The 2-mode model partially addresses the problem by only allowing it to affect the attribution of the deep mode, while the shallow mode is attributed to SC only.

However, our conclusion that regional hydrological sensitivity is mainly associated with $\partial P^*/\partial SC$ rather than $\partial P^*/\partial SST_{rel}$ is consistent with dynamical considerations. He et al. (2024) showed that tropical precipitation changes are determined by changes in boundary layer moist static energy, which are a function of ∂SST and changes in boundary layer relative humidity ($\partial RH0$). Therefore, regional hydrological sensitivity ($\partial P/\partial SST$) is primarily set by $\partial RH0$; the latter results from changes in boundary layer moisture transport driven by ∂SC (Supplementary Fig. 5, modified from He et al. 2024).

We derive constraints on $\partial P^*/\partial SST_{rel}$ and $\partial P^*/\partial SC$ based on the finding that the relationship between P* and SST_{rel} and that between P* and SST gradients remain approximately the same in a warm climate. This means that changes in SST geographically reshuffles P*, while the sensitivity of P* to SST_{rel} and SST gradient changes is determined by the climatological SST-precipitation relationship of each basin. Therefore, efforts to constrain regional hydrological sensitivity should focus on improving models' present-day SST-precipitation and SC-precipitation relationships.

Acknowledgement

We thank Drs. Robin Chadwick, Brian Soden and Bosong Zhang for helpful discussions. J.H. is supported by the National Science Foundation (NSF) grant AGS-2047270, B.F. is supported by NSF grant AGS-2217619, and Y.D. is supported by NSF grant AGS-2032532 and by the National Oceanic and Atmospheric Administration (NOAA) through Grants NA20OAR4310380 and NA22OAR4310606. We acknowledge the World Climate Research Programme's Working Group on Coupled Modelling, which is responsible for CMIP, and we thank the climate modelling groups for producing and making available their model output. For CMIP, the US Department of Energy's Program for Climate Model Diagnosis and Intercomparison provides coordinating support and led development of software infrastructure in partnership with the Global Organization for Earth System Science Portals. We thank the Physical Sciences Laboratory (PSL) of the National Oceanic and Atmospheric Administration and the Goddard Earth Sciences Data and Information Services Center for providing precipitation observations. We thank the Copernicus program, PSL, and the National Center for Atmospheric Research for providing the reanalysis data.

Open Research

All observational and reanalysis data and the CMIP6 outputs used in this paper are publicly available at the following websites. CMIP6: https://esgf-node.llnl.gov/projects/cmip6/. GPCP: https://psl.noaa.gov/data/gridded/data.gpcp.html. CMAP: https://www.psl.noaa.gov//data/gridded/data.cmap.html. TRMM: https://disc.gsfc.nasa.gov/datasets/TRMM_3B43_7/summary. ERA5: https://cds.climate.copernicus.eu/cdsapp#!/dataset/reanalysis-era5-pressure-levels-monthly-means?tab=form. NCEP/DOE-II: https://psl.noaa.gov/data/gridded/data.ncep.reanalysis2.html. JRA-55: https://jra.kishou.go.jp/JRA-55/index_en.html. Scripts used to analyze data and generate plots are stored in the Zenodo online repository at https://zenodo.org/records/10840557.

References

Adler, R. F., Huffman, G. J., Chang, A., Ferraro, R., Xie, P.-P., Janowiak, J., et al. (2003). The Version-2 Global Precipitation Climatology Project (GPCP) Monthly Precipitation Analysis (1979–Present). *Journal of Hydrometeorology*, *4*(6), 1147–1167. https://doi.org/10.1175/1525-7541(2003)004<1147:TVGPCP>2.0.CO;2

Back, L. E., & Bretherton, C. S. (2009a). A simple model of climatological rainfall and vertical motion patterns over the tropical oceans. *Journal of Climate*, *22*(23), 6477–6497.

Back, L. E., & Bretherton, C. S. (2009b). On the Relationship between SST Gradients, Boundary Layer Winds, and Convergence over the Tropical Oceans. *Journal of Climate*, *22*(15), 4182–4196. https://doi.org/10.1175/2009JCLI2392.1

Chadwick, R. (2016). Which Aspects of CO2 Forcing and SST Warming Cause Most Uncertainty in Projections of Tropical Rainfall Change over Land and Ocean? *Journal of Climate*, *29*(7), 2493–2509. https://doi.org/10.1175/JCLI-D-15-0777.1

Chen, X., Zhou, T., Wu, P., Guo, Z., & Wang, M. (2020). Emergent constraints on future projections of the western North Pacific Subtropical High. *Nature Communications*, *11*(1), 2802.

Conn, A. R., Gould, N. I., & Toint, P. L. (2000). *Trust region methods*. SIAM.

DeAngelis, A. M., Qu, X., Zelinka, M. D., & Hall, A. (2015). An observational radiative constraint on hydrologic cycle intensification. *Nature*, *528*(7581), 249–253. https://doi.org/10.1038/nature15770

Duffy, M. L., O'Gorman, P. A., & Back, L. E. (2020). Importance of Laplacian of Low-Level Warming for the Response of Precipitation to Climate Change over Tropical Oceans. *Journal of Climate*, *33*(10), 4403–4417. https://doi.org/10.1175/JCLI-D-19-0365.1

Eyring, V., Bony, S., Meehl, G. A., Senior, C. A., Stevens, B., Stouffer, R. J., & Taylor, K. E. (2016). Overview of the Coupled Model Intercomparison Project Phase 6 (CMIP6) experimental design and organization. *Geoscientific Model Development*, *9*(5), 1937–1958.

Good, P., Chadwick, R., Holloway, C., Kennedy, J., Lowe, J., Roehrig, R., & Rushley, S. (2020). High sensitivity of tropical precipitation to local sea-surface temperature.

Graham, N. E., & Barnett, T. P. (1987). Sea Surface Temperature, Surface Wind Divergence, and Convection over Tropical Oceans. *Science*, *238*(4827), 657. https://doi.org/10.1126/science.238.4827.657

Ham, Y.-G., Kug, J.-S., Choi, J.-Y., Jin, F.-F., & Watanabe, M. (2018). Inverse relationship between present-day tropical precipitation and its sensitivity to greenhouse warming. *Nature Climate Change*, *8*(1), 64–69. https://doi.org/10.1038/s41558-017-0033-5

He, J., & Soden, B. J. (2015). Anthropogenic Weakening of the Tropical Circulation: The Relative Roles of Direct CO2 Forcing and Sea Surface Temperature Change. *Journal of Climate*, *28*(22), 8728–8742. https://doi.org/10.1175/JCLI-D-15-0205.1

He, J., Johnson, N. C., Vecchi, G. A., Kirtman, B., Wittenberg, A. T., & Sturm, S. (2018). Precipitation Sensitivity to Local Variations in Tropical Sea Surface Temperature. *Journal of Climate*, *31*(22), 9225–9238. https://doi.org/10.1175/JCLI-D-18-0262.1

He, J., Lu, K., Fosu, B., & Fueglistaler, S. (2024). Diverging Hydrological Sensitivity among Tropical Basins. Nature Climate Change, Accepted.

Hersbach, H., Bell, B., Berrisford, P., Hirahara, S., Horányi, A., Muñoz-Sabater, J., et al. (2020). The ERA5 global reanalysis. *Quarterly Journal of the Royal Meteorological Society*, *146*(730), 1999–2049.

Huffman, G. J., Adler, R. F., Bolvin, D. T., & Nelkin, E. J. (2010). The TRMM multi-satellite precipitation analysis (TMPA). In *Satellite rainfall applications for surface hydrology* (pp. 3–22). Springer.

Hurrell, J. W., Hack, J. J., Shea, D., Caron, J. M., & Rosinski, J. (2008). A new sea surface temperature and sea Ice boundary dataset for the community atmosphere model. *Journal of Climate*, *21*(19), 5145–5153. https://doi.org/10.1175/2008JCLI2292.1

Johnson, N. C., & Xie, S.-P. (2010). Changes in the sea surface temperature threshold for tropical convection. *Nature Geosci*, *3*(12), 842–845. https://doi.org/10.1038/ngeo1008

Kanamitsu, M., Ebisuzaki, W., Woollen, J., Yang, S.-K., Hnilo, J., Fiorino, M., & Potter, G. (2002). Ncep–doe amip-ii reanalysis (r-2). *Bulletin of the American Meteorological Society*, *83*(11), 1631–1644.

Kent, C., Chadwick, R., & Rowell, D. P. (2015). Understanding uncertainties in future projections of seasonal tropical precipitation. *Journal of Climate*, *28*(11), 4390–4413. https://doi.org/10.1175/JCLI-D-14-00613.1

KOBAYASHI, S., OTA, Y., HARADA, Y., EBITA, A., MORIYA, M., ONODA, H., et al. (2015). The JRA-55 Reanalysis: General Specifications and Basic Characteristics. *気象集誌. 第 2 輯*, *93*(1), 5–48. https://doi.org/10.2151/jmsj.2015-001

Kramer, R. J., & Soden, B. J. (2016). The sensitivity of the hydrological cycle to internal climate variability versus anthropogenic climate change. *Journal of Climate*, *29*(10), 3661–3673.

Lau, K.-M., Wu, H.-T., & Bony, S. (1997). The Role of Large-Scale Atmospheric Circulation in the Relationship between Tropical Convection and Sea Surface Temperature. *Journal of Climate*, *10*(3), 381–392. https://doi.org/10.1175/1520-0442(1997)010<0381:TROLSA>2.0.CO;2

Lindzen, R. S., & Nigam, S. (1987). On the Role of Sea Surface Temperature Gradients in Forcing Low-Level Winds and Convergence in the Tropics. *Journal of the Atmospheric Sciences*, *44*(17), 2418–2436. https://doi.org/10.1175/1520-0469(1987)044<2418:OTROSS>2.0.CO;2

Lu, K., He, J., & Simpson, I. R. (2023). Origins of uncertainty in the response of the summer north Pacific subtropical high to CO2 forcing. *Geophysical Research Letters*, *50*(22), e2023GL105042.

Ma, J., & Xie, S.-P. (2013). Regional patterns of sea surface temperature change: a source of uncertainty in future projections of precipitation and atmospheric circulation. *Journal of Climate*, *26*(8), 2482–2501. https://doi.org/10.1175/JCLI-D-12-00283.1

McSweeney, C. F., & Jones, R. G. (2013). No consensus on consensus: the challenge of finding a universal approach to measuring and mapping ensemble consistency in GCM projections. *Climatic Change*, *119*(3), 617–629. https://doi.org/10.1007/s10584-013-0781-9

Neelin, J. D., & Held, I. M. (1987). Modeling Tropical Convergence Based on the Moist Static Energy Budget. *Monthly Weather Review*, *115*(1), 3–12. https://doi.org/10.1175/1520-0493(1987)115<0003:MTCBOT>2.0.CO;2

Park, I.-H., Yeh, S.-W., Min, S.-K., Ham, Y.-G., & Kirtman, B. P. (2022). Present-day warm pool constrains future tropical precipitation. *Communications Earth & Environment*, *3*(1), 310.

Su, H., Jiang, J. H., Neelin, J. D., Shen, T. J., Zhai, C., Yue, Q., et al. (2017). Tightening of tropical ascent and high clouds key to precipitation change in a warmer climate. *Nature Communications*, *8*, 15771.

Watanabe, M., Kamae, Y., Shiogama, H., DeAngelis, A. M., & Suzuki, K. (2018). Low clouds link equilibrium climate sensitivity to hydrological sensitivity. *Nature Climate Change*, *8*(10), 901–906. https://doi.org/10.1038/s41558-018-0272-0

Xie, P., & Arkin, P. A. (1997). Global Precipitation: A 17-Year Monthly Analysis Based on Gauge Observations, Satellite Estimates, and Numerical Model Outputs. *Bulletin of the American Meteorological Society*, *78*(11), 2539–2558. https://doi.org/10.1175/1520-0477(1997)078<2539:GPAYMA>2.0.CO;2

Xie, S.-P., Deser, C., Vecchi, G. A., Ma, J., Teng, H., & Wittenberg, A. T. (2010). Global Warming Pattern Formation: Sea Surface Temperature and Rainfall. *Journal of Climate*, *23*(4), 966–986. https://doi.org/10.1175/2009JCLI3329.1

Zhang, C. (1993). Large-Scale Variability of Atmospheric Deep Convection in Relation to Sea Surface Temperature in the Tropics. *Journal of Climate*, *6*(10), 1898–1913. https://doi.org/10.1175/1520-0442(1993)006<1898:LSVOAD>2.0.CO;2

Zhang, J., & Huang, P. (2023). Different uncertainty in tropical oceanic and land precipitation sensitivities under global warming. *Atmospheric Research*, 106850.

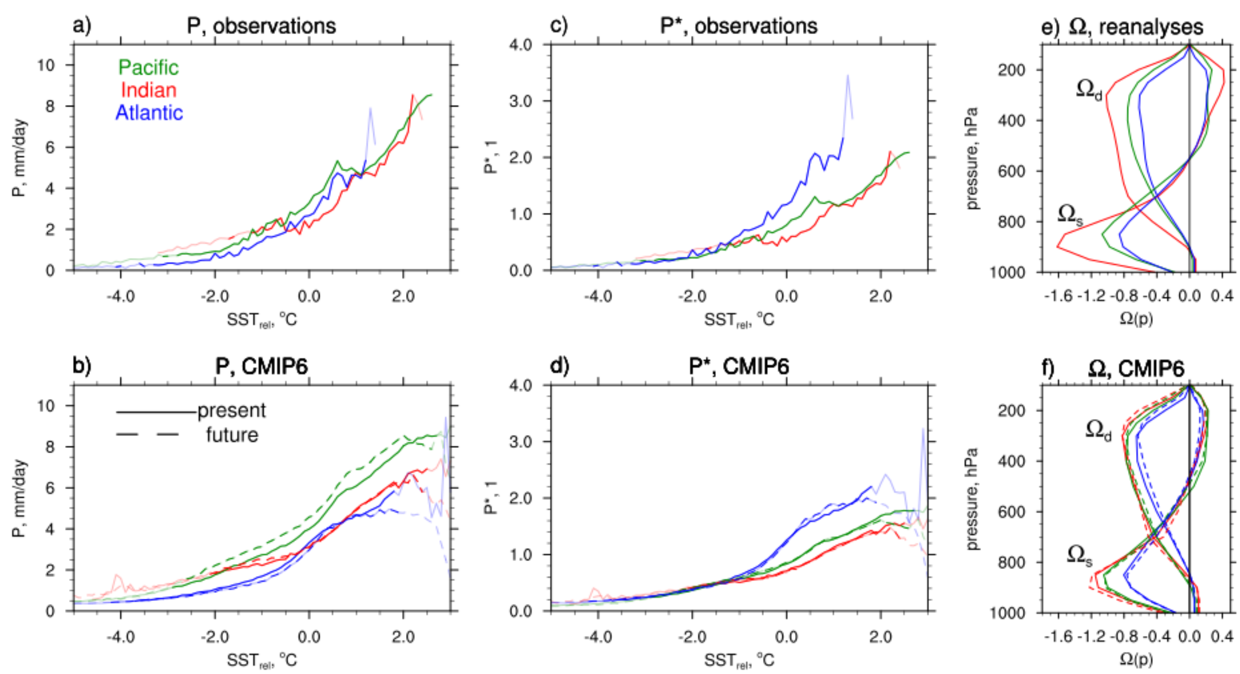

Figure 1. a-b) Basin precipitation averaged for 0.1 SST_{rel} bins from observations (a) and CMIP6 multi-model mean historical and ssp585 simulations (b). SST_{rel} bins that account for less than 0.5%

of the basin area are shown in semitransparent colors. c-d) Same as a-b) but for relative precipitation. e-f) Vertical profiles of deep and shallow pressure velocity profiles from reanalysis (e) and CMIP6 multi-model mean historical and ssp585 simulations (f).

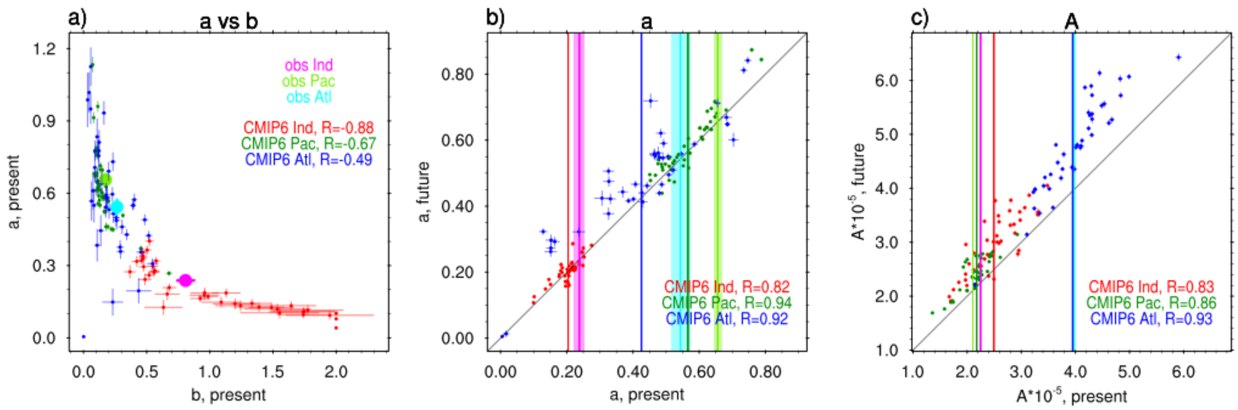

Figure 2. Relationships between present-day *a* and *b* (a), present-day and future *a* (b), and present-day and future *A* (c). Individual GCMs are represented by the small dots, and the vertical lines in (b) and (c) represent the multi-model mean. Inter-model correlation coefficients are shown by texts. Observations are represented by the large dots in (a) vertical lines in (b) and (c) in lighter colors. The 95% uncertainty range is represented by the crosses for the individual GCMs in all panels and observations in (a) and is represented by the semitransparent shading for the observations in (b) and (c).

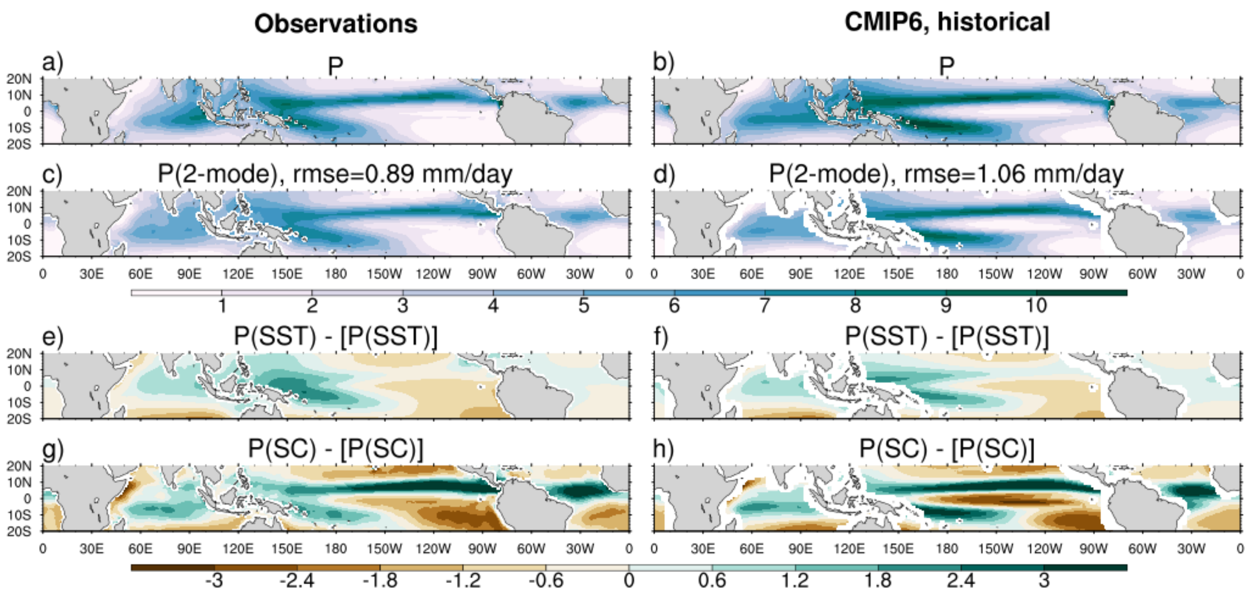

Figure 3. Present-day precipitation (a-b), estimated precipitation by the 2-mode model (c-d), and SST-driven and SC-driven precipitation (e-h) from the observations (left) and the CMIP6 multi-model mean (right). The 2-mode model estimates P* and P is obtained by multiplying P* by the observed or GCMs' [P]. In (e-h), the basin mean P(SST) and P(SC) are removed in order to emphasize their spatial variations.

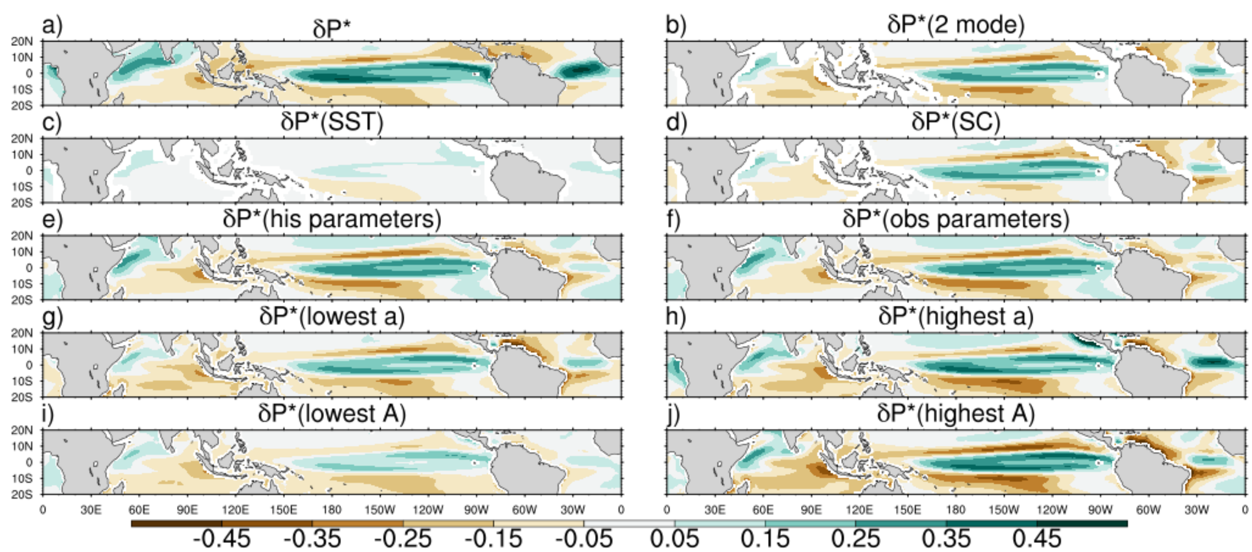

Figure 4. a-b) CMIP6 multi-model mean P* changes from GCMs (a) and the 2-mode model (b). c-d) Multi-model mean P* changes due to changes in SST (c) and SC (d). e-f) Multi-model mean P* changes from the 2-mode model by using GCMs' historical parameters (e) and observational parameters (f). g-h) Same as (b) except replacing parameter a of all GCMs with those from GCMs with the lowest a (g) and highest a (h). i-j) Same as (g-h) except for parameter A.